CSMA 2017
13ème Colloque National en Calcul des Structures
15-19 Mai 2017, Presqu'île de Giens (Var)

A continuum formulation of the finite strain equilibrium gap regularizer for finite element image correlation problems

M. Genet[1], L. C. Lee[2], S. Kozerke[3]

[1] *Laboratoire de Mécanique des Solides, École Polytechnique, Palaiseau (martin.genet@polytechnique.edu)*
[2] *Michigan State University, East Lansing, USA (lclee@egr.msu.edu)*
[3] *ETH Zurich, Switzerland (kozerke@biomed.ee.ethz.ch)*

Résumé —
This abstract briefly describes a novel continuum finite strain formulation of the equilibrium gap principle, introduced in (CLAIRE, HILD et ROUX, 2004) at the discrete level for linearized elasticity, used as a regularizer for finite element-based image correlation problems. Consistent linearization and finite element discretization is provided. The method is implemented using FEniCS & VTK, in a freely available python library. The equilibrium gap constraint regularizes the image correlation problem, even in presence of noise, and without affecting strain measurement.
Mots clés — Finite elements, Image Correlation, Equilibrium Gap Regularization, Hyperelasticity.

1 Context

Image processing, in particular image correlation/registration, is playing an increasing role in many domains such as mechanical (BORNERT et al., 2009) and biomedical (TOBON-GOMEZ et al., 2013 ; LEE et al., 2014) engineering. Despite important progress in the past decades, robustness, efficiency and precision of existing methods and tools must still be improved to translate them into medical and engineering applications. This abstract briefly describes a novel continuum finite strain formulation of the equilibrium gap principle, introduced in (CLAIRE, HILD et ROUX, 2004) at the discrete level for linearized elasticity and further developed for instance in (LECLERC et al., 2010), as a regularizer for finite element-based image correlation problems.

2 Problem

Let us denote I_0 & I_t as the intensity fields of two images representing an object occupying the domains Ω_0 & Ω_t in the reference and deformed states, respectively. The problem is to find the mapping $\underline{\varphi}$ between Ω_0 & Ω_t, or equivalently the displacement field $\underline{U}$ ($\underline{\varphi}(\underline{X}) = \underline{X} + \underline{U}(\underline{X})$), which is reformulated as a minimization problem written in the reference configuration :

$$\text{find } \underline{U} = \text{argmin}_{\{\underline{U}^*\}} \left\{ J^2(\underline{U}^*) = \frac{1-\beta}{2} \int_{\Omega_0} \left(I_t \circ \underline{\varphi}^* - I_0 \right)^2 d\Omega_0 + \beta \psi^{\text{reg}}(\underline{U}^*) \right\}, \tag{1}$$

where ψ^{reg} is required to regularize the otherwise ill-posed problem, and β is the regularization strength. Many regularizers have been proposed, including fluid (CHRISTENSEN, RABBITT et MILLER, 1996) and hyperelastic (VERESS, GULLBERG et WEISS, 2005 ; PHATAK et al., 2009 ; GENET, STOECK et al., 2016) constraints. Hyperelastic warping consists in using the strain energy potential directly as regularizer :

$$\psi^{\text{reg,hyper}} = \rho_0 \psi, \tag{2}$$

thus penalizing strain. Here we propose an alternate regularizer, which essentially penalizes any deviation from the solution of an hyperelastic body in equilibrium with arbitrary external loads : $\psi^{\text{reg,equil}} = \frac{1}{2} \left\| \underline{\text{div}}\left(\underline{\underline{P}}\right) \right\|^2_{L^2(\Omega_0)}$, where $\underline{\underline{P}} = \frac{\partial \rho_0 \psi}{\partial \underline{\underline{F}}}$ is the first Piola-Kirchhoff stress tensor. However, we discretize Problem (1) using standard Lagrange elements, so that $\underline{\underline{P}}$ belongs to $L^2(\Omega_0)$ but not $H(\text{div};\Omega_0)$. Thus, the

following equivalent norm is used instead :

$$\psi^{\text{reg,equil}} = \sum_K \frac{1}{2} \left\| \underline{\text{div}}\left(\underline{\underline{P}}\right) \right\|^2_{L^2(K)} + \sum_F \frac{1}{2h} \left[\left[\underline{\underline{P}} \cdot \underline{N}\right]\right]^2_{L^2(K)}, \tag{3}$$

where K denotes the set of finite elements, F the set the interior faces, h a characteristic length of the mesh. As strain energy function, for both hyperelastic and equilibrated warping we use the classical Ciarlet-Geymonat (CIARLET et GEYMONAT, 1982) potential :

$$\rho_0\psi = \frac{\kappa}{2}\left(J^2 - 1 - \ln(J)\right) + \frac{\mu}{2}\left(I_C - 3 - 2\ln(J)\right), \tag{4}$$

where κ & μ denote bulk and shear modulus, $J = \det\left(\underline{\underline{F}}\right)$, $I_C = \text{tr}\left(\underline{\underline{C}}\right)$, $\underline{\underline{C}} = {}^t\underline{\underline{F}} \cdot \underline{\underline{F}}$, $\underline{\underline{F}} = \underline{\underline{1}} + \underline{\underline{\text{grad}}}\left(\underline{U}\right)$, and which makes sense for arbitrary deformation levels (LE TALLEC, 1994). In practice, we use a unit Young's modulus and null Poisson's ratio, so that $\kappa = \frac{1}{3}$ & $\mu = \frac{1}{2}$, the strength of the regularization being set by the parameter β.

3 Variational formulation

After derivation and linearization, Problem (1) becomes :

$$\text{find } \underline{\Delta U} \;/\; (1-\beta)\, a^{\text{cor}}\left(\underline{U};\underline{\Delta U},\underline{V}\right) + \beta a^{\text{reg}}\left(\underline{U};\underline{\Delta U},\underline{V}\right) = (1-\beta)\, b^{\text{cor}}\left(\underline{U};\underline{V}\right) + \beta b^{\text{reg}}\left(\underline{U};\underline{V}\right) \forall \underline{V}, \tag{5}$$

where (without image hessian terms)

$$\left\{\begin{array}{l} a^{\text{cor}}\left(\underline{U};\underline{\Delta U},\underline{V}\right) = \displaystyle\int_{\Omega_0} \left(\left(\underline{\nabla I_1} \circ \underline{\varphi}\left(\underline{U}\right)\right) \cdot \underline{\Delta U}\right) \left(\left(\underline{\nabla I_1} \circ \underline{\varphi}\left(\underline{U}\right)\right) \cdot \underline{V}\right) d\Omega_0 \\ b^{\text{cor}}\left(\underline{U};\underline{V}\right) = \displaystyle\int_{\Omega_0} \left(\left(I_1 \circ \underline{\varphi}\left(\underline{U}\right)\right) - I_0\right) \left(\left(\underline{\nabla I_1} \circ \underline{\varphi}\left(\underline{U}\right)\right) \cdot \underline{V}\right) d\Omega_0 \end{array}\right. \tag{6}$$

In case of hyperelastic warping, one has :

$$\left\{\begin{array}{l} a^{\text{reg,hyper}}\left(\underline{U};\underline{\Delta U},\underline{V}\right) = \displaystyle\int_{\Omega_0} \frac{\partial \rho_0\psi}{\partial \underline{\underline{E}}}\left(\underline{U}\right) : \underline{\underline{\delta E}}\left(\underline{\Delta U},\underline{V}\right) + \underline{\underline{\delta E}}\left(\underline{U},\underline{\Delta U}\right) : \frac{\partial^2 \rho_0\psi}{\partial \underline{\underline{E}}^2}\left(\underline{U}\right) : \underline{\underline{\delta E}}\left(\underline{U},\underline{V}\right) d\Omega_0 \\ b^{\text{reg,hyper}}\left(\underline{U};\underline{V}\right) = \displaystyle\int_{\Omega_0} \frac{\partial \rho_0\psi}{\partial \underline{\underline{E}}}\left(\underline{U}\right) : \underline{\underline{\delta E}}\left(\underline{U},\underline{V}\right) d\Omega_0 \end{array}\right. \tag{7}$$

And in case of equilibrated warping, one has :

$$\left\{\begin{array}{l} a^{\text{reg,equil}}\left(\underline{U};\underline{\Delta U},\underline{V}\right) = \displaystyle\sum_K \int_K \underline{\text{div}}\left(\underline{\underline{F}}\left(\underline{\Delta U}\right) \cdot \frac{\partial \rho_0\psi}{\partial \underline{\underline{E}}}\left(\underline{U}\right) + \underline{\underline{F}}\left(\underline{U}\right) \cdot \left(\frac{\partial^2 \rho_0\psi}{\partial \underline{\underline{E}}^2}\left(\underline{U}\right) : \underline{\underline{\delta E}}\left(\underline{U},\underline{\Delta U}\right)\right)\right) \\ \qquad \cdot \underline{\text{div}}\left(\underline{\underline{F}}\left(\underline{V}\right) \cdot \frac{\partial \rho_0\psi}{\partial \underline{\underline{E}}}\left(\underline{U}\right) + \underline{\underline{F}}\left(\underline{U}\right) \cdot \left(\frac{\partial^2 \rho_0\psi}{\partial \underline{\underline{E}}^2}\left(\underline{U}\right) : \underline{\underline{\delta E}}\left(\underline{U},\underline{V}\right)\right)\right) \\ \qquad + \underline{\text{div}}\left(\underline{\underline{F}}\left(\underline{U}\right) \cdot \frac{\partial \rho_0\psi}{\partial \underline{\underline{E}}}\left(\underline{U}\right)\right) \cdot \underline{\text{div}}\left(\underline{\underline{F}}\left(\underline{V}\right) \cdot \left(\frac{\partial^2 \rho_0\psi}{\partial \underline{\underline{E}}^2}\left(\underline{U}\right) : \underline{\underline{\delta E}}\left(\underline{U},\underline{\Delta U}\right)\right) + \underline{\underline{F}}\left(\underline{\Delta U}\right) \cdot \left(\frac{\partial^2 \rho_0\psi}{\partial \underline{\underline{E}}^2}\left(\underline{U}\right) : \underline{\underline{\delta E}}\left(\underline{U},\underline{V}\right)\right)\right. \\ \qquad \left. + \underline{\underline{F}}\left(\underline{U}\right) \cdot \left(\underline{\underline{\delta E}}\left(\underline{U},\underline{\Delta U}\right) : \frac{\partial^3 \rho_0\psi}{\partial \underline{\underline{E}}^3}\left(\underline{U}\right) : \underline{\underline{\delta E}}\left(\underline{U},\underline{V}\right) + \frac{\partial^2 \rho_0\psi}{\partial \underline{\underline{E}}^2}\left(\underline{U}\right) : \underline{\underline{\delta E}}\left(\underline{\Delta U},\underline{V}\right)\right)\right) dK \\ + \displaystyle\sum_F \int_F \left[\left[\left(\underline{\underline{F}}\left(\underline{\Delta U}\right) \cdot \frac{\partial \rho_0\psi}{\partial \underline{\underline{E}}}\left(\underline{U}\right) + \underline{\underline{F}}\left(\underline{U}\right) \cdot \left(\frac{\partial^2 \rho_0\psi}{\partial \underline{\underline{E}}^2}\left(\underline{U}\right) : \underline{\underline{\delta E}}\left(\underline{U},\underline{\Delta U}\right)\right)\right) \cdot \underline{N}\right]\right] \\ \qquad \cdot \left[\left[\left(\underline{\underline{F}}\left(\underline{V}\right) \cdot \frac{\partial \rho_0\psi}{\partial \underline{\underline{E}}}\left(\underline{U}\right) + \underline{\underline{F}}\left(\underline{U}\right) \cdot \left(\frac{\partial^2 \rho_0\psi}{\partial \underline{\underline{E}}^2}\left(\underline{U}\right) : \underline{\underline{\delta E}}\left(\underline{U},\underline{V}\right)\right)\right) \cdot \underline{N}\right]\right] \\ + \left[\left[\left(\underline{\underline{F}}\left(\underline{U}\right) \cdot \frac{\partial \rho_0\psi}{\partial \underline{\underline{E}}}\left(\underline{U}\right)\right) \cdot \underline{N}\right]\right] \cdot \left[\left[\left(\underline{\underline{F}}\left(\underline{V}\right) \cdot \left(\frac{\partial^2 \rho_0\psi}{\partial \underline{\underline{E}}^2}\left(\underline{U}\right) : \underline{\underline{\delta E}}\left(\underline{U},\underline{\Delta U}\right)\right) + \underline{\underline{F}}\left(\underline{\Delta U}\right) \cdot \left(\frac{\partial^2 \rho_0\psi}{\partial \underline{\underline{E}}^2}\left(\underline{U}\right) : \underline{\underline{\delta E}}\left(\underline{U},\underline{V}\right)\right)\right.\right. \\ \qquad \left.\left. + \underline{\underline{F}}\left(\underline{U}\right) \cdot \left(\underline{\underline{\delta E}}\left(\underline{U},\underline{\Delta U}\right) : \frac{\partial^3 \rho_0\psi}{\partial \underline{\underline{E}}^3}\left(\underline{U}\right) : \underline{\underline{\delta E}}\left(\underline{U},\underline{V}\right) + \frac{\partial^2 \rho_0\psi}{\partial \underline{\underline{E}}^2}\left(\underline{U}\right) : \underline{\underline{\delta E}}\left(\underline{\Delta U},\underline{V}\right)\right)\right) \cdot \underline{N}\right]\right] dF \\ b^{\text{reg,equil}}\left(\underline{U};\underline{V}\right) = \displaystyle\sum_K \int_K \underline{\text{div}}\left(\underline{\underline{F}}\left(\underline{U}\right) \cdot \frac{\partial \rho_0\psi}{\partial \underline{\underline{E}}}\left(\underline{U}\right)\right) \cdot \underline{\text{div}}\left(\underline{\underline{F}}\left(\underline{V}\right) \cdot \frac{\partial \rho_0\psi}{\partial \underline{\underline{E}}}\left(\underline{U}\right) + \underline{\underline{F}}\left(\underline{U}\right) \cdot \left(\frac{\partial^2 \rho_0\psi}{\partial \underline{\underline{E}}^2}\left(\underline{U}\right) : \underline{\underline{\delta E}}\left(\underline{U},\underline{V}\right)\right)\right) dK \\ \qquad + \displaystyle\sum_F \int_F \left[\left[\left(\underline{\underline{F}}\left(\underline{U}\right) \cdot \frac{\partial \rho_0\psi}{\partial \underline{\underline{E}}}\left(\underline{U}\right)\right) \cdot \underline{N}\right]\right] \cdot \left[\left[\left(\underline{\underline{F}}\left(\underline{V}\right) \cdot \frac{\partial \rho_0\psi}{\partial \underline{\underline{E}}}\left(\underline{U}\right) + \underline{\underline{F}}\left(\underline{U}\right) \cdot \left(\frac{\partial^2 \rho_0\psi}{\partial \underline{\underline{E}}^2}\left(\underline{U}\right) : \underline{\underline{\delta E}}\left(\underline{U},\underline{V}\right)\right)\right) \cdot \underline{N}\right]\right] dF \end{array}\right. \tag{8}$$

4 Resolution

Problem (5) is discretized using continuous Galerkin elements, and solved in FEniCS [1]. Integration of image terms (6) is done using VTK [2]. Code is freely available at `https://bitbucket.org/mgenet/dolfin_dic`.

Since the resolution has proven unstable on *in vivo* images (especially because *(i)* in current VTK implementation, interpolated gradients are not the actual gradients of the interpolated images [3] ; and *(ii)* the mechanical term is very steep), a gradient-free golden section line search has been implemented, where the initial interval is taken as $\left[\frac{1-\varphi}{2-\varphi};\frac{1}{2-\varphi}\right]$ (with $\varphi=\frac{1+\sqrt{5}}{2}$) such that the two initially tested values are 0 & 1.

5 Results on synthetic data

Here we consider the simple problem of a uniformly deforming square domain, and study the influence of the regularization strength β on the computed strain. Figure 1 shows the initial and final images with superimposed undeformed and deformed mesh, for three levels of noise, as well as the final measured strain for both methods.

In case of hyperelastic warping, if the regularization strength is close to 1, the mesh does not deform. And when regularization strength decreases, measured strain tends to converge toward the exact value. For noise-free images, it does converge exactly. For noisy images, there is an optimum where the mean strain is close to the exact solution and standard deviation is still limited.

Conversely, with equilibrated warping, the registration is almost perfect, over a wide range of regularization strengths, even on noisy images.

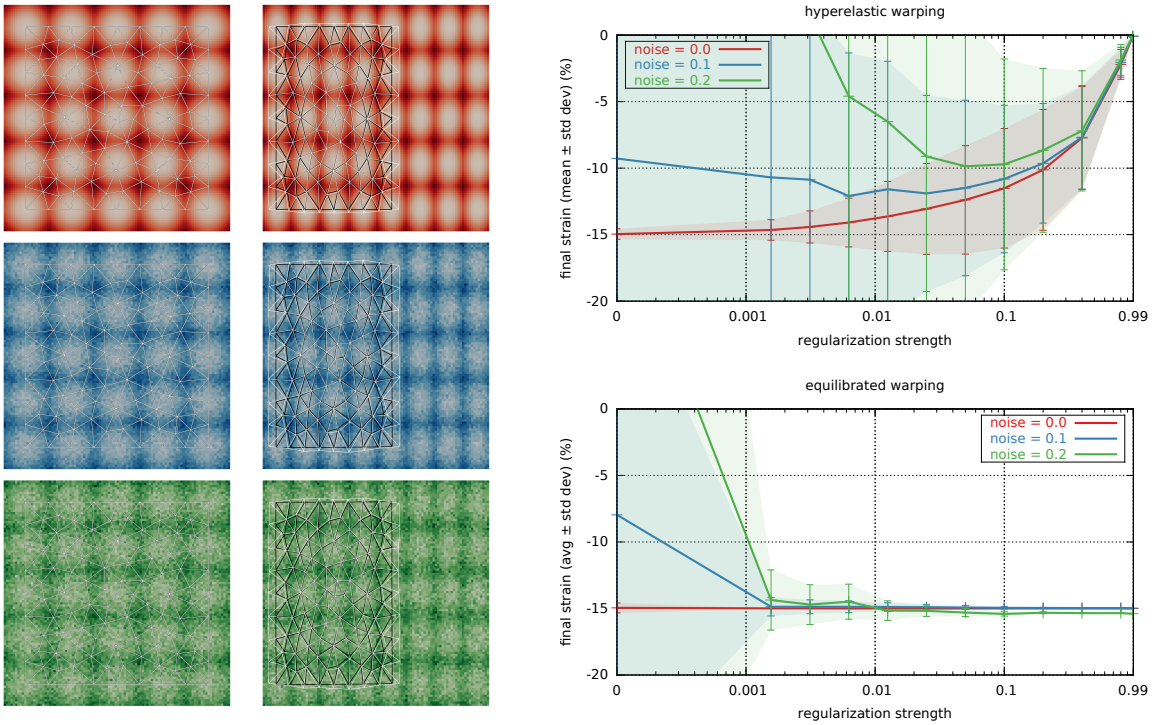

FIGURE 1 – Results on synthetic data. Left : hyperelastic (white mesh) *vs.* equilibrated (black mesh) warping, for a regularization strength of 0.1. Right : influence of regularization strength on hyperelastic (top) and equilibrated (bottom) warping strains. Ground truth is -15% homogeneous strain.

1. `https://fenicsproject.org`
2. `http://www.vtk.org`
3. `http://www.vtk.org/Wiki/VTK/Image_Interpolators\#Gradients`

6 Results on *in vivo* images

Here we consider 3DCSPAMM (STOECK et al., 2012) cardiac magnetic resonance images of a healthy human subject. Pipeline for image acquisition and segmentation has been described in (GENET, LEE, NGUYEN et al., 2014 ; GENET, LEE, GE et al., 2015). Figure 2 shows the resulting strains computed by both methods. Main features of left ventricular deformation are well captured, including radial thickening as well as circumferential and longitudinal shortening, though radial strains are somewhat smaller than expected, as has already been noted in (TOBON-GOMEZ et al., 2013). Equilibrated warping produces larger absolute strain values than hyperelastic warping, closer to expected values (TOBON-GOMEZ et al., 2013).

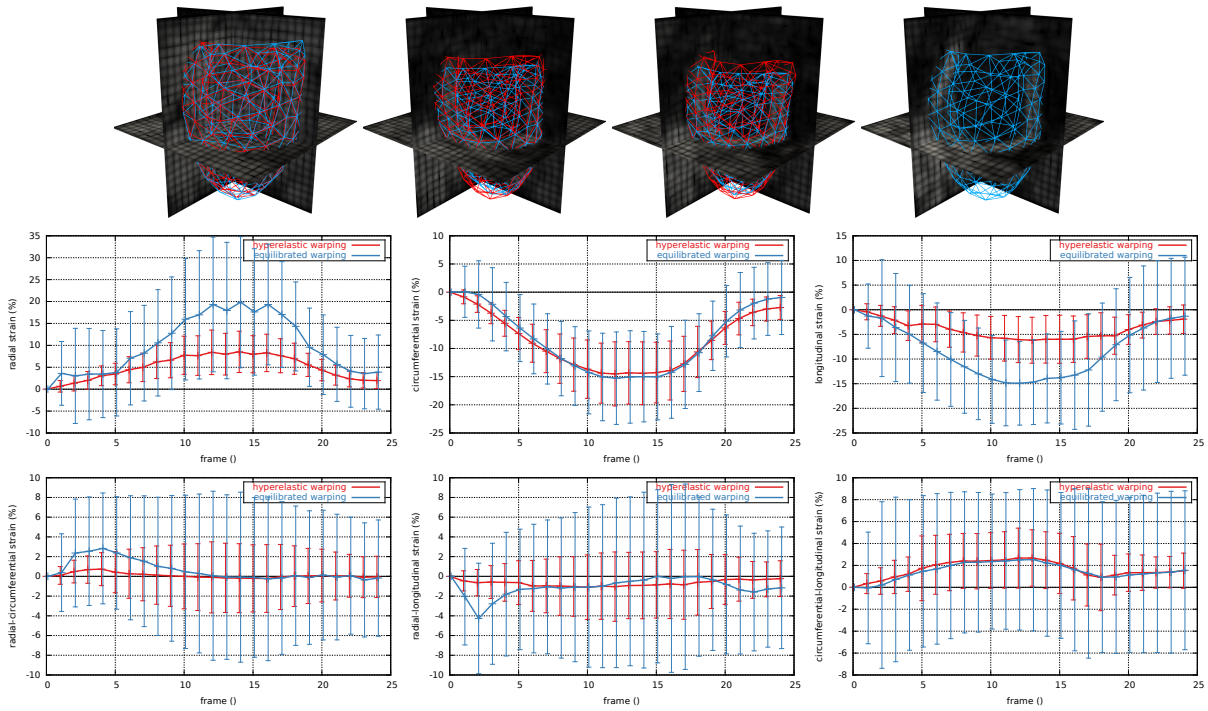

FIGURE 2 – Results on *in vivo* data, hyperelastic (red) *vs.* equilibrated (blue) warping. Top : Sequence of 3D CSPAMM images with superimposed mesh. Bottom : Sequence of local strain components.

7 Conclusion

Equilibrated warping is a powerful method for non-rigid registration of images involving large deformation. The equilibrium gap constraint regularizes the image correlation problem, even in presence of noise, and without affecting strain measurement. The method has been implemented based on FEniCS and VTK, providing an efficient tool for 2D & 3D images registration.

Références

BORNERT, M. et al. (2009). “Assessment of Digital Image Correlation Measurement Errors : Methodology and Results”. In : *Experimental Mechanics* 49.3. 00344, p. 353–370.

CHRISTENSEN, G. E., R. D. RABBITT et M. I. MILLER (1996). “Deformable Templates Using Large Deformation Kinematics”. In : *IEEE transactions on image processing : a publication of the IEEE Signal Processing Society* 5.10. 01275, p. 1435–47.

CIARLET, P. G. et G. GEYMONAT (1982). “Sur Les Lois de Comportement En Élasticité Non-Linéaire Compressible”. In : *Comptes Rendus de l’Académie des Sciences Série II* 295, p. 423–426.

CLAIRE, D., F. HILD et S. ROUX (2004). “A Finite Element Formulation to Identify Damage Fields : The Equilibrium Gap Method”. In : *International Journal for Numerical Methods in Engineering* 61.2. 00164, p. 189–208.

GENET, M., L. C. LEE, L. GE et al. (2015). “A Novel Method for Quantifying Smooth Regional Variations in Myocardial Contractility Within an Infarcted Human Left Ventricle Based on Delay-Enhanced Magnetic Resonance Imaging”. In : *Journal of Biomechanical Engineering* 137.8.

GENET, M., L. C. LEE, R. NGUYEN et al. (2014). “Distribution of Normal Human Left Ventricular Myofiber Stress at End Diastole and End Systole : A Target for in Silico Design of Heart Failure Treatments.” In : *Journal of Applied Physiology* 117, p. 142–52.

GENET, M., C. T. STOECK et al. (2016). “Finite Element Digital Image Correlation for Cardiac Strain Analysis from 3D Whole-Heart Tagging”. In : *24rd Annual Meeting of the International Society for Magnetic Resonance in Medicine (ISMRM2016)*.

LE TALLEC, P. (1994). “Numerical Methods for Nonlinear Elasticity”. In : *Handbook of Numerical Analysis*. T. 3. 00167, p. 465–622.

LECLERC, H. et al. (2010). “Voxel-Scale Digital Volume Correlation”. In : *Experimental Mechanics* 51.4. 00080, p. 479–490.

LEE, L. C. et al. (2014). “Applications of Computational Modeling in Cardiac Surgery”. In : *Journal of Cardiac Surgery* 29.3, p. 293–302.

PHATAK, N. S. et al. (2009). “Strain Measurement in the Left Ventricle during Systole with Deformable Image Registration”. In : *Medical image analysis* 13.2. 00000, p. 354–61.

STOECK, C. T. et al. (2012). “Undersampled Cine 3D Tagging for Rapid Assessment of Cardiac Motion”. In : *Journal of Cardiovascular Magnetic Resonance* 14.1. 00009, p. 60.

TOBON-GOMEZ, C. et al. (2013). “Benchmarking Framework for Myocardial Tracking and Deformation Algorithms : An Open Access Database”. In : *Medical Image Analysis* 17.6. 00057, p. 632–648.

VERESS, A. I., G. T. GULLBERG et J. A. WEISS (2005). “Measurement of Strain in the Left Ventricle during Diastole with Cine-MRI and Deformable Image Registration”. In : *Journal of Biomechanical Engineering* 127.7, p. 1195.